JACS
JOURNAL OF THE AMERICAN CHEMICAL SOCIETY

Article

Non-Covalent Interactions Drive the Efficiency of Molybdenum Imido Alkylidene Catalysts for Olefin Metathesis

Marco Antonio Barbosa Ferreira, Jordan De Jesus Silva, Samantha Grosslight, Alexey Fedorov, Matthew S Sigman, and Christophe Copéret

J. Am. Chem. Soc., **Just Accepted Manuscript** • DOI: 10.1021/jacs.9b04367 • Publication Date (Web): 10 Jun 2019

Just Accepted

is published by the American Chemical Society. 1155 Sixteenth Street N.W., Washington, DC 20036

Non-Covalent Interactions Drive the Efficiency of Molybdenum Imido Alkylidene Catalysts for Olefin Metathesis

Marco A. B. Ferreira,*[,†,§] Jordan De Jesus Silva,[‡] Samantha Grosslight,[†] Alexey Fedorov,*[,‡,¶] Matthew S. Sigman,*[,†] Christophe Copéret*[,‡]

[†]Department of Chemistry, University of Utah, 315 South 1400 East, Salt Lake City, Utah 84112, United States

[‡]Department of Chemistry and Applied Biosciences, ETH Zürich, Vladimir-Prelog-Weg 1-5, CH-8093 Zürich, Switzerland

[§]Department of Chemistry, Federal University of São Carlos – UFSCar, Rodovia Washington Luís, km 235, SP-310, São Carlos, São Paulo, Brazil, 13565-905

[¶] Department of Mechanical and Process Engineering, ETH Zürich, Leonhardstrasse 21, CH-8092 Zürich, Switzerland

ABSTRACT: High-throughput experimentation and multivariate modelling allow identification of non-covalent interactions (NCIs) in monoaryloxy-pyrrolide Mo imido alkylidene metathesis catalysts prepared *in situ* as a key driver for high activity in a representative cross-metathesis reaction (homodimerization of 1-nonene). Statistical univariate and multivariate modelling categorizes catalytic data from 35 phenolic ligands into two groups, depending on the substitution in the *ortho* position of the phenol ligand. Catalytic activity descriptor TON_{1h} correlates predominantly with attractive NCIs when *ortho* aryl phenols are used and, conversely, with repulsive NCIs when the phenol has no aryl *ortho* substituents. Energetic span analysis is deployed to relate the observed NCI and the cycloreversion metathesis step such that aryloxide ligands with no *ortho* aryls mainly impact the energy of metallacyclobutane intermediates (SP/TBP isomers), whereas aryloxides with pendant *ortho* aryls influence the transition state energy for the cycloreversion step. While the electronic effects from the aryloxide ligands also play a role, our work outlines how NCIs may be exploited for the design of improved d^0 metathesis catalysts.

INTRODUCTION

Transition-metal-catalyzed olefin metathesis has over the last decades transformed the pharmaceutical, polymer, and fine chemicals industries.[1] Among the various systems available, Schrock-type Mo and W d^0 alkylidenes[2] have been developed into highly active, selective and stable metathesis catalysts, with performance metrics that are attractive for industrial applications.[3] Recent compelling developments include metal imido alkylidene complexes (X)(Y)M(=NR)(=CHR[1]) with different X and Y ligand set (M = Mo, W; X ≠ Y, and X is a stronger σ-donor), for instance the monoaryloxy pyrrolide (MAP)[2,4] and monoaryloxy chloride (MAC)[5] family of catalysts, that enable the selective synthesis of (*Z*)-alkenes, including chloro and fluoroalkenes. The dissymmetry at the metal center of such catalysts was recognized early as an important factor associated with enhanced metathesis activity.[6] Metallacyclobutanes (MCB), the key intermediates of the Chauvin mechanism of olefin metathesis,[7] are proposed through computational studies to adopt a 5-coordinate trigonal-bipyramidal (TBP) geometry with the X – typically more σ-donating – group and the metallacycle in the equatorial plane (Scheme 1A).[6] Such TBP intermediates can however undergo a turnstile isomerization process yielding an off-cycle MCB with a square-based pyramidal (SP) geometry that slows down catalysis and promotes deactivation and side-reactions.[6a-d,8,9,10] The presence of σ-donor ligands with varying donation properties in these unsymmetrical catalysts raises the energy of metallacyclobutane intermediates preventing their overstabilization.[6b-d] Overall, this suggests that the effectiveness of an alkene metathesis reaction could be improved by minimizing the concentration of an off-cycle SP metallacycle, however, the rational design of Schrock-type metathesis catalysts remains challenging and often unpredictable.

Herein, we describe a high-throughput experimental (HTE) approach to identify active, *in-situ*-generated molybdenum alkylidene complexes tested for a

prototypical cross metathesis reaction, the homodimerization of 1-nonene, that is plagued with deactivation pathways associated with the formation of ethylene, and that requires a better understanding of key parameters driving this reaction.[6a,d,11] The HTE methodology is integrated with multivariate statistical modelling strategies that guide the search for highly efficient catalysts and provide insights on key parameters for further catalyst design (Scheme 1B,C). We evaluated *in situ* formulations prepared from a library of 35 phenols and two precursor bis-pyrrolido complexes,[12] targeting both unsymmetrical MAP and symmetrical bisaryloxide families of complexes, prepared using 1:1 and 2:1 ratios of ArOH and $(2,5\text{-}(Me)_2\text{-}Pyr)_2Mo(=NAr)(=CHCMe_2Ph)$, respectively [Ar = 2,6-(iPr)$_2$-Ph (**Mo-1**) and 2,6-(Me)$_2$-Ph (**Mo-2**)].

Scheme 1. The mechanism of olefin metathesis with d^0 catalysts (A), design of the HTE study (B, C) and catalytic results (D) for *in situ* formulations of **Mo-1** with ArOH **1**-**35** in 1:1 ratio (Pyr = 2,6-dimethylpyrrolido). *Because of the increasing amounts of isomerization products after the complete consumption of 1-nonene, TON values are reported after 75 minutes and 135 minutes instead of 75 minutes and 501 minutes.

A. Proposed catalytic cycle with d⁰ (X)(Y)M(=E)(=CHR¹) catalysts for alkene metathesis

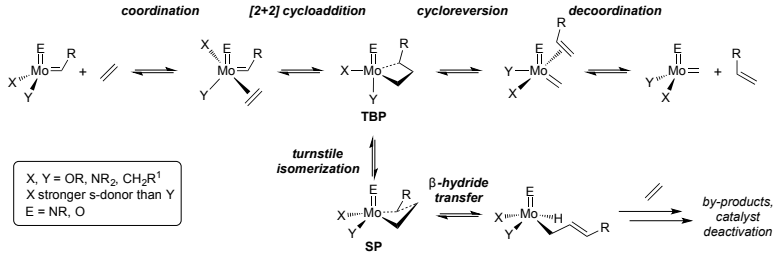

B. *In-situ*-generated molybdenum alkylidene complexes for homodimerization of 1-nonene (steps 1-2)

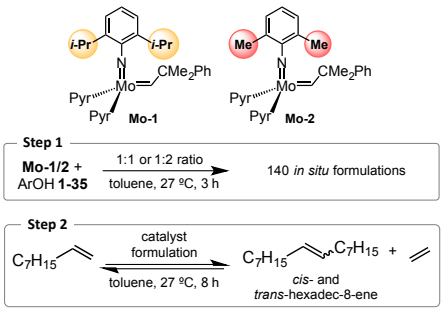

C. Library of phenol ligands

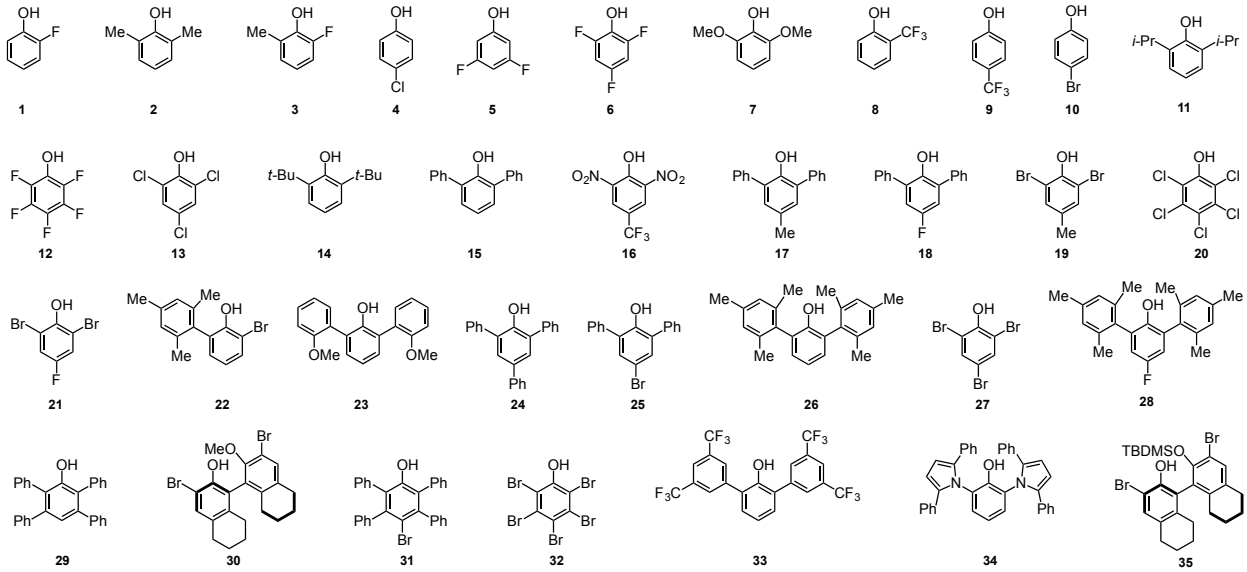

D. Results for the catalytic homodimerization of 1-nonene with formulations prepared from Mo-1 and ArOH-1-35 (1:1 ratio, see ESI for details)

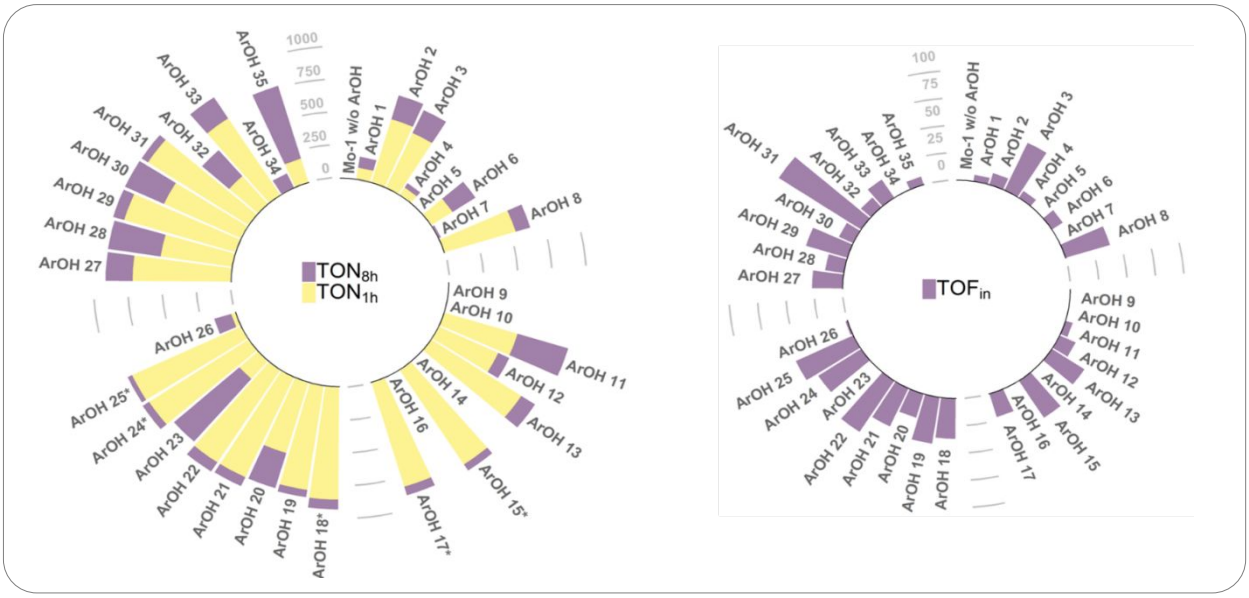

The resulting dependence of both the productive (i.e., calculated from the yield of the C_{16} products) turnover number (TON) and turnover frequency (TOF) was quantitatively related to structural features of aryloxy ligands by examining their computed electronic and steric characteristics using multivariate regression

analysis.[13] The resultant statistical models provide a correlation between a non-covalent interaction (NCI) exerted by phenolic ligands and productive TONs and TOFs. Ultimately, the results could be interpreted with respect to the stability of the TBP and SP intermediates and respective transition states for the cycloreversion step, furnishing guidelines for predictable catalyst design.

RESULTS AND DISCUSSION

Testing *in situ* Prepared Mo Metathesis Catalysts in the Homodimerization of 1-Nonene

Phenol ligands **1**-**35** were selected for catalytic testing due to their broad range of electronic and steric properties, while also possessing common characteristics that could facilitate identification of uncorrelated structural features essential for catalytic performance. For simplicity, ArOH are numbered according to their increasing molecular weight. Formulations were prepared *in situ* from molybdenum bispyrrolide precursors **Mo-1** and **Mo-2** and ligands **1**-**35** (Scheme 1B,C) by stirring 1 or 2 equiv. of the phenol with a respective Mo-precursor in toluene for 3 hours at 27 °C. An aliquot of each mixture was combined with 1-nonene to deliver a 1000/1 substrate-to-catalyst ratio (0.1 mol % catalyst loading). These steps were performed by an automated liquid handling robotic system operated inside an inert atmosphere glovebox (see ESI for details). The reaction mixtures were agitated for ca. 8 hours at 27 °C in open vials,[14] and reaction progress was monitored by GC after ca. 6, 16, 39, 72, 135, 258 and 501 minutes, giving conversions (*X*), selectivity for the formation of hexadec-8-ene (S_{C16} and $S_{C16}(E/Z)$), and respective turnover numbers and turnover frequencies. These data are presented in the ESI (Tables S3-6) including conversion vs. time and *E/Z* selectivity vs. time plots (Figures S18-159). Robustness tests were routinely performed in triplicate with new batches of 1-nonene, exhibiting good reproducibility (Tables S7-8). Below, the discussion is focused on two selected responses, namely productive TOF_{in} and TON_{1h} (data points collected after ca. 6 and 72 min, respectively). The first response reflects the initial activity of the catalyst formulation, wherein the influence of catalyst deactivation is minimal. While no formulation reaches complete conversion of 1-nonene after 1 h, several formulations feature conversion exceeding 90 %, and in general X_{1h} > 50% at this reaction time (Scheme 1D). Therefore, TON_{1h} was used as a response to evaluate the overall catalyst efficiency comprising both activity and stability as it allows us to differentiate each catalyst's efficiency that is not possible with later time points since many formulations reach complete conversion making these measurements insensitive for discriminating between catalysts. Examples of outputs for productive TOF_{in}, TON_{1h} and TON_{8h} obtained with 1:1 ratio of **Mo-1** and ArOH **1-35** are presented in Scheme 1D (see ESI for such plots using 1:2 ratio and results with **Mo-2**, Figures S3-5).

Inspection of TOF_{in} and TON_{1h} for 1:1 and 1:2 formulations with either **Mo-1** or **Mo-2** reveals high collinearity (R^2 = 0.79 – 0.97) of these reactivity outputs (Figures S13-14). In contrast, comparing TOF_{in} and TON_{1h} values for 1:1 formulation relative to both arylimido ligands uncovers noteworthy differences. *In situ* formulations derived from **Mo**-**2**, a precursor with a smaller 2,6-dimethylphenylimido ligand relative to 2,6-diisopropylphenylimido ligand in **Mo-1**, exhibit significantly reduced TOF_{in} and TON_{1h} values using phenols that lack pendant aryl groups in *ortho* positions, with several phenols giving inactive formulations, in sharp contrast to **Mo**-**1** (Scheme 1D and Figures S15). However, phenols with pendant aryls display a high degree of collinearity for both Mo precursors. These observations point at significant influence of *ortho* aryl substituents on generating active catalyst formulations (*vide infra*). Remarkably, almost all active catalysts present high S_{C16} selectivity (averages of 95% and 93% at 1h and 8h, respectively).

Next, we sought to correlate activity and stability of *in situ* formulations with the structural characteristics of the tested phenol ligands. For brevity, we limit the discussion below primarily to results obtained using 1:1 ratio of **Mo-1** and phenols **1**-**35**. TOF_{in} and TON_{1h} values for these tests are reasonably correlated (R^2 = 0.67, Figure 1A), suggesting that most of the ligands are associated with similar deactivation pathways. Considering that 1-nonene concentration decreases over time, a drop in the reaction rate and consequently TOF_{1h} < TOF_{in} were expected. To identify ligands furnishing higher catalytic stability, we defined a deactivation parameter as DEACT = $[(TOF_{1h} - TOF_{in})/TOF_{in}] \times 100\%$ that revealed a typical range for deactivation across most of tested phenols at 65-90%. However, bulky phenols **2**, **17**, **23**, **27**, **28**, **30**, and **33** give more stable formulations with **Mo-1**, deactivating to a significantly lower extent (20-55%). Hexadec-8-ene forms faster at 1 h relative to the initial rate only for one example, the bulky phenol **11**. This result is due to a slow induction period observed at the beginning of the reaction with **11**. Thus, the DEACT parameter identifies the most stable formulations, as well as induction periods (observed only for ArOH-**11**).

In general, the (*E*/*Z*) ratios for the S_{C16} (*E*) isomer increase with reaction progress for most formulations and catalysts typically display $S_{C16}(E/Z)_{8h}$ >4 if TON_{8h} exceeds ca. 850, especially for formulations with **Mo**-**1** (Figure 1B). This is consistent with the competing metathesis isomerization that is favored for the more active and stable catalysts as these systems are likely to

display a *E*/*Z* ratio approaching the thermodynamic value at higher conversions. Only the bulky ligands **26**, **33**, **34**, and **35** do not follow this trend and favor the formation of *cis*-hexadec-8-ene, in line with previous reports demonstrating that homocoupling[3] and cross-metathesis[4] of terminal alkenes could proceed in high *Z*-selectivity with bulky MAP catalysts.

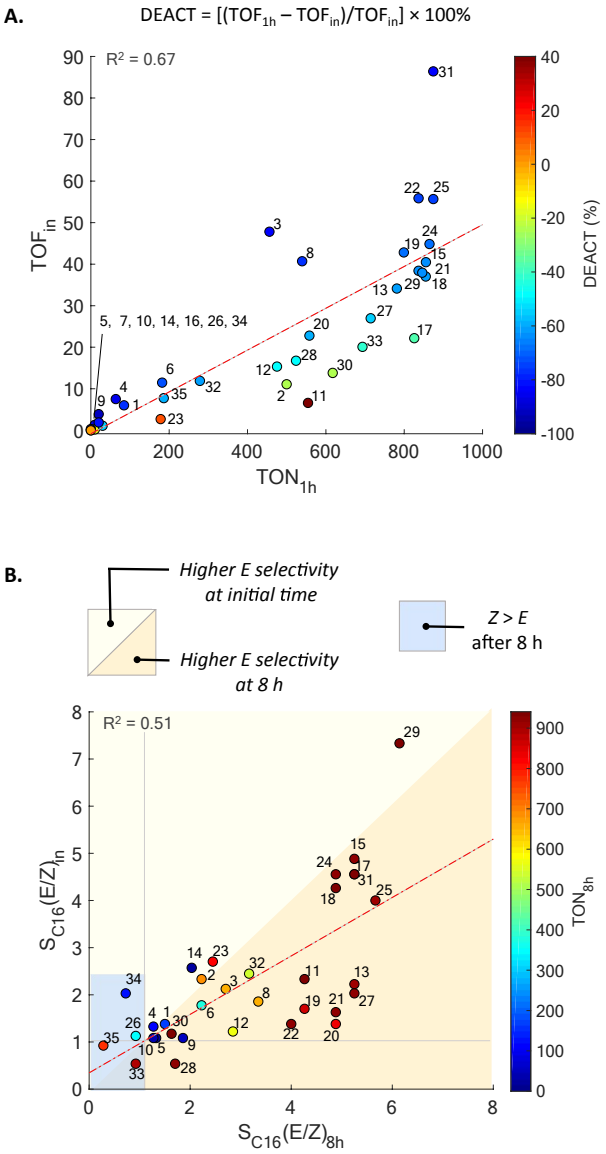

Figure 1. Analysis of experimental descriptors obtained with 1:1 *in situ* formulations with ligands **1**-**35** and **Mo-1**.

While well-defined metathesis catalysts with large aryloxy ligands typically produce high TONs and reaction rates,[4,5,9] *in situ* formulations with bulky ligands **15**, **26**, **29**, **30** and **35** do not follow a clear trend, with **Mo-1** giving TON_{1h} of 860, 110, 850, 620 and 190, respectively; the TON_{1h} values are also similar with **Mo-2** (Figure 2A). Notably, these high TON values highlight that the exchange of bispyrrolido for aryloxy ligands proceeds under these conditions even with rather bulky phenols as ArOH **29**, **30** and **35**. Furthermore, evaluation of the homologous series of tri- and penta-halogenated phenols (**6**, **12**, **13**, **20**, **27**, and **32**) with **Mo-1** and **Mo-2** reveals that the more electronegative ligands display lower TON_{1h} values (Figure 2B). The fluorophenols **6** and **12** are less electronegative than chloro- and bromophenols (**13**, **20**, **27**, **32**) and based on the above result might be expected to feature high TON_{1h} as well. However, the most electropositive phenol **6** yields the lowest TON_{1h} in this series, possibly due to the intermolecular ligand scrambling forming respective bispyrrolides and bisaryloxides.[15] Overall, this points to an entangled influence of phenol structural properties on catalyst activity, which in turn hampers rational design of metathesis catalysts.

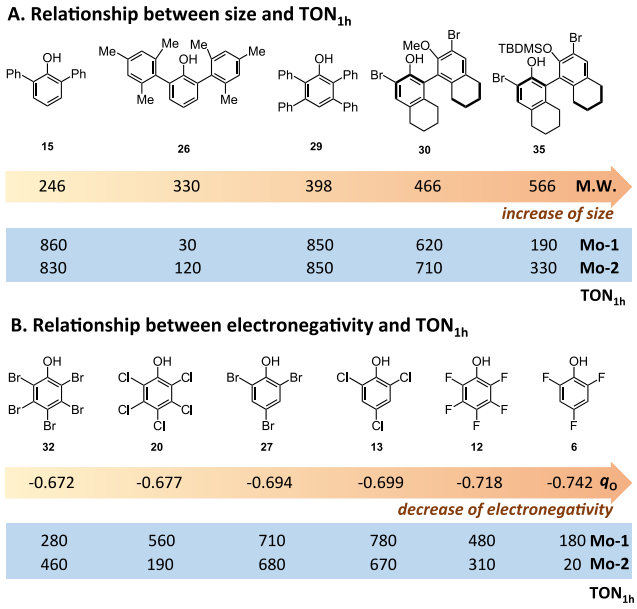

Figure 2. Preliminary analysis of structural features of selected phenol ligands and catalytic activity of formulations derived from **Mo-1** and **Mo-2**. The estimates for size and electronegativity were molecular weight (MW) and natural bond orbital (NBO) charges of the oxygen (q_O of phenolate), respectively.

Parametrization

Considering the lack of obvious trends between catalytic activity and structural features of phenols, we chose to apply statistical correlation tools to classify TOF_{in} and TON_{1h} data using approaches evolving from the Sigman group.[16] Our general workflow to correlate these reaction outputs to molecular descriptors of phenolic ligands included a variety of calculated steric and electronic molecular parameters (Figure 3A). First, a conformational ensemble of relevant geometries was generated using Molecular Mechanics (MM), followed by DFT geometry optimization to identify the lowest energy conformer at

the M06-2X/def2-TZVP level of theory, which provides the platform to assemble structural parameters for further analysis. Subsequently, a preliminary identification of univariate trends and application of multivariate linear regression analysis provide statistical models required for interrogation of the origin of olefin metathesis efficiency of the *in situ* formulations. In particular, we highlight below the development of statistical models based on new tailored steric probes (calculated at B97-D3/def2-TZVP level of theory).

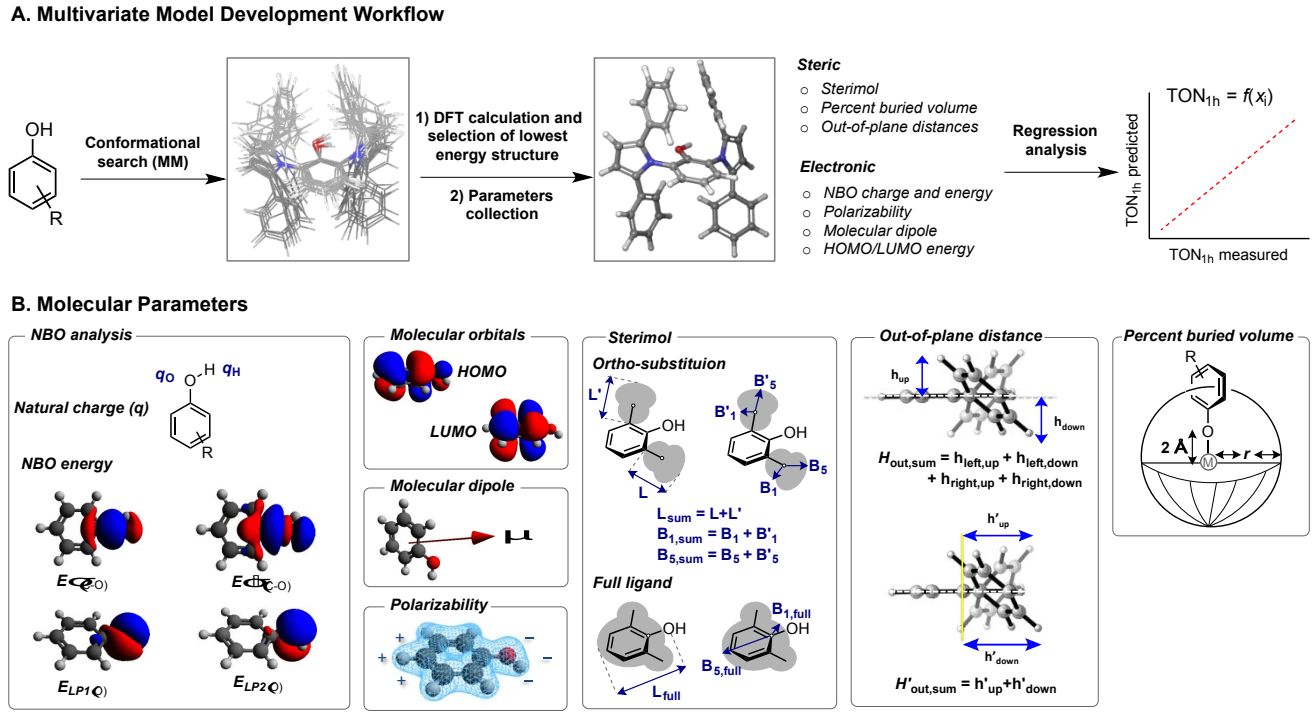

Figure 3. Parameterization of phenol ligands: development workflow of multivariate models (A) and selected calculated molecular parameters (B).

Descriptors of Phenol Ligands

Electronic Descriptors. The electron density of each free phenol ligand or phenolate anion were assessed relative to natural bond orbital (NBO) charges of oxygen (q_O),[17] C–O bonding $\sigma_{(C\text{-}O)}$ ($E\sigma_{(C\text{-}O)}$) and antibonding $\sigma^*_{(C\text{-}O)}$ ($E\sigma^*_{(C\text{-}O)}$) NBO energies (Figure 3B). Additional parameters included HOMO/LUMO energies, NBO energies of lone pairs of oxygen $E_{LP(O)}$, molecular dipole (μ), and polarizability (*Pol*). These values are presented in the supporting information.

Steric Descriptors. The steric influence of phenol ligands was initially assessed using Verlop's Sterimol parameters.[18] We considered individually the two pendant groups in the *ortho* position (L, B_1, B_5, L', B'_1, B'_5), using the sum of both as the final parameter (Figure 3B). In a second approach, we subjected the entire phenol to the Sterimol calculation. Additionally, we investigated alternative steric parameters including the height above a defined plane, labelled as $H_{out,sum}$ and $H'_{out,sum}$.[19] These parameters account for the steric effects caused by 2,6-substituents of the phenol ring; additional parameters are presented in ESI. Finally, the percent buried volume ($\%V_{bur}$) was determined, which is defined as the fraction of the volume occupied by a ligand in an abstract sphere centered on the metal atom.[20] The set radius sphere of r = 5.0 Å was selected to capture the steric influence of the *meta* substituent of the phenol ring; lower r values (3.5 and 4.0 Å) allow selectively capturing steric effects of *ortho* substituents.

Preliminary Correlation Analysis

At this stage, we considered all tested phenol ligands that had improved activity of the precursor complex **Mo-1**, seeking to relate their electronic and steric properties to experimental TOF_{in} and TON_{1h} values. An initial univariate correlation matrix, represented as a color map in Figure 4A, was generated, revealing only low R^2 values not exceeding 0.22. A more detailed analysis of the univariate trend of TOF_{in} with the best correlating parameter, L_{sum}, showed two distinct sets of catalysts that differ by the presence or absence of aryl substituents in *ortho* positions of respective phenol ligands (Figure 4B). Therefore, we categorized the data set into two distinct subsets: Group A contains phenols without aryl arms in the *ortho* position (**1**-**14**, **16**, **19**-**21**, **27**, **32**) and Group B contains *ortho*-arylated phenols (**15**, **17**-**18**, **22**-**26**, **28**-**31**, **33**-**35**). These improved individual univariate correlations using several steric descriptors of phenol ligands and TOF_{in} and TON_{1h} values (R^2 in the range of

0.5-0.9; see Figures S16-S17 in ESI). For example, a statistically significant correlation was observed for 1:1 formulations with **Mo-1** in Group A using the size of the phenolic substituents represented by the $\%V_{bur}$ steric descriptor (Figure 4C). Interestingly, a correlation of Group B ligands with the same measure reveals an inverted correlation, wherein the larger phenols are associated with reduced activity. Considering that the $\%V_{bur}$ captures the steric effect mainly of the *ortho* positions, these trends hint at the importance of NCIs exerted by these substituents with optimal radius spheres of r = 3.5 and 4.0 Å for Groups A and B, respectively.

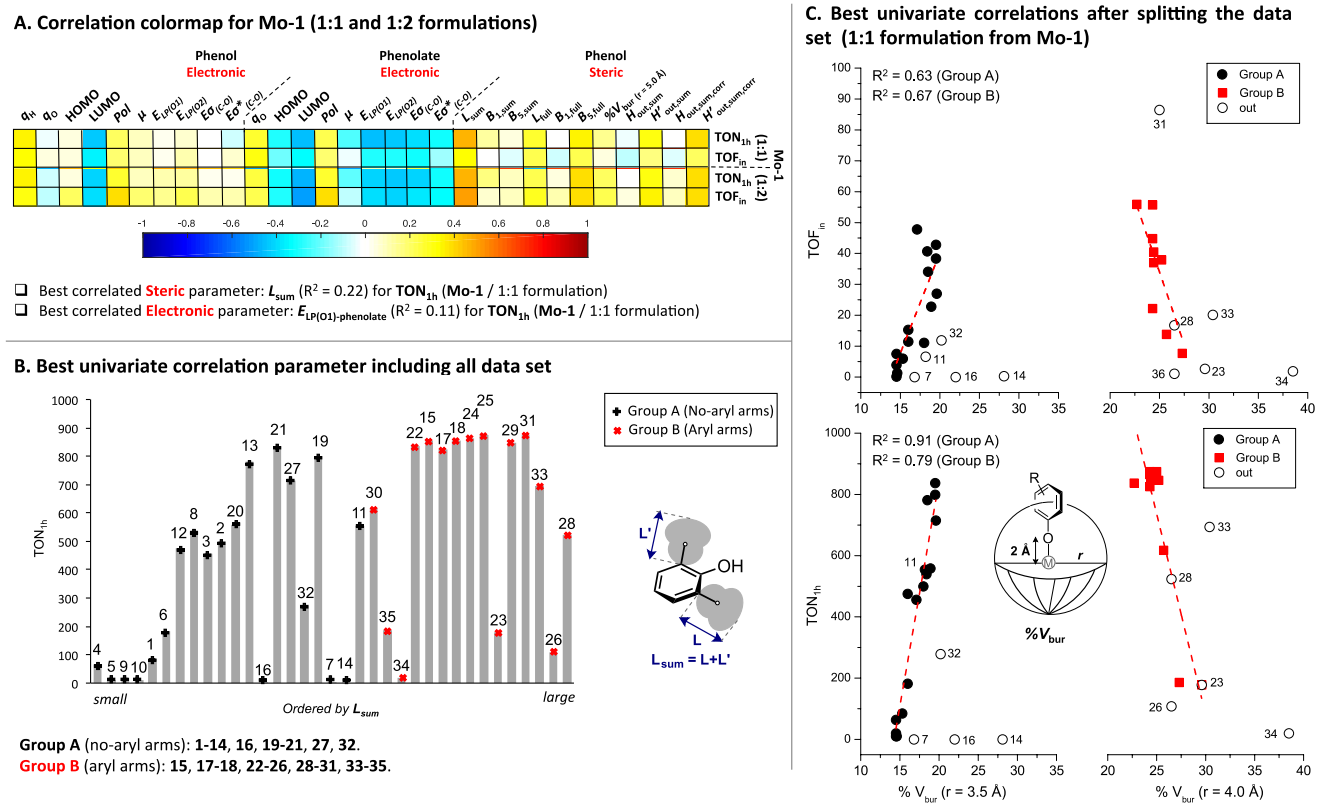

Figure 4. Initial correlation analysis. Correlation color map for formulations with **Mo-1** (A), optimal univariate steric correlation parameter (B), and best univariate correlation after splitting the data set into groups with and without *ortho* aryl substituents in phenols (C). The Group A contains phenols without aryl arms in the *ortho* position, and Group B contains *ortho*-arylated phenols.

Analysis of Outliers and Control Experiments

Some outliers were excluded from the correlations presented in Figure 4C. While 2,6-(i-Pr)$_2$-PhOH (**11**) yields a formulation with a comparable productive TON_{1h} to 2,6-(Me)$_2$-PhOH (**2**) (500 and 540, respectively), the initial calculation of $\%V_{bur}$ is likely overestimated for **11**, which we attribute to conformational differences of this aryloxide in the Mo complex and the free ligand. The conformer is shown in Figure S7 in the supporting information, and has one of the C–Me bonds eclipsed by the aromatic ring, driving the second methyl group towards the oxygen of the phenolate, thereby overestimating the steric effect of the i-Pr group in $\%V_{bur}$ parameter. In contrast, in **11** or related complexes Mo(NAr)($CH_2CH_2CH_2$)(Me_2Pyr)L,[6c] the C–H bond is eclipsed by the aromatic ring and directed to the oxygen of the phenol, increasing the distance between the CH_3 group and the metal center. In order to obtain a more reliable $\%V_{bur}$ value of **11**, we fixed the dihedral C_A–C_{Ar}–C–H angle to 0°, which allows this data point to be accurately incorporated into the correlation. However, **11** remains an outlier in TOF_{in} correlation due to the slow induction period, as identified by the DEACT parameter (Figure 1A).

Others outliers were the pentabromophenol **32**, and the [2,6-(3,5-(CF_3)$_2$-Ph)$_2$-PhOH] **33,** which combines rather large substituents with significant electronic perturbation on the aromatic system. This strongly suggests the required inclusion of electronic terms in the statistical modeling.

A special group of outliers with lower activity was found to directly relate to slow ligand exchange when forming

the active catalysts. For example, combining **Mo-1** and 2,6-(*t*-Bu)$_2$-PhOH (**14**) of Group A leaves **Mo-1** unreacted at room temperature according to ^{1}H NMR (see Figure S6 in ESI for more details). This is presumably due to the large size of this phenol retarding the substitution reaction. For similar reasons, the complete ligand exchange of **Mo-1** with 2,6-(Mes)$_2$- derivatives **26** (2,6-(Mes)$_2$-PhOH) and **28** (2,6-(Mes)$_2$-4-F-PhOH) of Group B requires longer reaction time (Figure S6). Likewise, the bulky ligand **34** [2,6-(2,5-Ph-Pyr)$_2$-PhOH] showed the lowest catalytic performance in Group B giving <5% of the ligand exchange product after ca. 1 day.

Finally, two particular cases of low-activity catalysts were identified in both groups and involved 2,6-(OMe)$_2$-PhOH (**7**) and 2,6-(2-OMe-Ph)$_2$-PhOH (**23**) phenols. Both yield a stable 1:1 complex as determined by *in situ* NMR experiments, avoiding the exchange of a second aryloxy ligand when a second equivalent of **7** or **23** was added (Figure S6). Therefore, their low activities are presumably due the coordination between the methoxy substituent on the ligand and the metal center (MeO–Mo interaction).

Electronic Correlations of *Ortho*-Isosteric Ligands

To explore the electronic impact of ligand **32** and related phenols in our correlations, we evaluated a series of phenols with the same *ortho* substituents and selected phenols with the 2,6-(Br)$_2$- and 2,6-(Ph)$_2$- ligands (**19**, **21**, **27**, **32** from Group A, and **15**, **17**, **18**, **24**, **25**, **29**, **31** from Group B). Figure 5 depicts good univariate inter-correlations found for these sub-classes of phenols. Analysis of 2,6-(Br)$_2$- ligands demonstrates an excellent correlation of TOF_{in} and the NBO charge of the phenol oxygen (q_O; greater negative values represents a more electron rich aromatic ring, see Table S14 of SI) associating a reduction in TOF_{in} with an increase in electronegativity (Figure 5A). The latter could also be interpreted as decrease in σ-donating properties of the aryloxy ligand, which is expected to stabilize the TBP intermediate relative to the off-cycle SP isomer, as was already discussed above. Similarly, a good correlation is observed for the TON_{1h} response with the *Pol* parameter (R^2 = 0.97) (Figure 5B), which may be understood as a hybrid descriptor, and potentially directly related to dispersive stabilizing forces. It is noteworthy that more electronegative substituents in the aromatic system raise the polarization of the π-system, which in this case lowers catalytic performance (TOF_{in}).

Likewise, analysis of the 2,6-(Ph)$_2$- series of phenols reveals a divergent scenario. These phenols demonstrate that increasing the electronegativity (weaker σ-donor ligands) enhances the rates as defined by a strong correlation between TOF_{in} and q_O (R^2 = 0.93, Figure 5C). Similarly, a good correlation (R^2 = 0.83) between TON_{1h} and C–O bonding $\sigma_{(C\text{-}O)}$ NBO energies ($E\sigma_{(C\text{-}O)}$; directly associated with the electronic density of the aromatic ring, with less negative values representing electron rich aromatic rings, see Table S14 of ESI) was observed.

Overall, the data suggest that electronic influences are more substantial at the initial phase of the reaction, while the effect of ligand size is influential as the reaction progresses, ultimately impacting catalyst stability as assessed by TON_{1h}. This is found for both Groups A and B, confirmed by the higher collinearity between TON_{1h} and $\%V_{Bur}$ (Figure 4C).

Development of Steric Probes for Non-Covalent Interactions (NCIs)

The rational development of catalysts[21] has often relied on the concept of steric repulsion. More recently, the importance of stabilizing non-covalent substrate–catalyst interactions has been recognized as central for the geometrical preorganization of transition states.[22] Although NCIs forces are individually relatively weak, they rapidly become important for molecular structures of increasing size.[23] Multivariate statistical modeling using NCIs as parameter has been reported.[23]

As suggested by the initial analysis detailed above, the correlations for **Mo-1** formulations as well as inferior performance of formulation derived from the smaller **Mo-2** precursor advocate that NCIs may be influencing the catalytic activity. We have therefore focused on developing probes more specific to NCI interactions and that can be used for statistical analyses. On the basis of reports by Bohm and Exner,[24] we exploited homodesmotic reactions[25] to derive NCI sensitive parameters using only one half of the phenol ligand to reduce the conformational complexity (Figure 6A). For non-symmetric ligands, we considered the sum of both sides of the phenol. All probes were normalized to Ph, that is defined as $\Delta E_{[Ph]} = 0$.

Our first probe, $\Delta E_{NCI\text{-}A}$ defined as presented in Figure 6A, aimed to capture the NCI exerted by the pendant groups in the *ortho* position of ArOH (Figure 6A). It should be noted though that the close proximity between the *ortho*-aryl substituents and the adamantyl group likely compromises reliability of this parameter for bulkier substituents like *t*-Bu, delivering values significantly higher than expected (Table S13). Thus, a second probe was designed, which avoids these issues. According to previous studies using 1,8-diarylnaphthalenes in this context,[26] the stabilizing π-stacking and CX---π (X = H, halogen) interactions exerted in the Mo complex by ligands with pendant aryl groups may be captured ($\Delta E_{NCI\text{-}}$

B, Figure 6A). This probe should provide a good balance between repulsive and attractive NCIs.

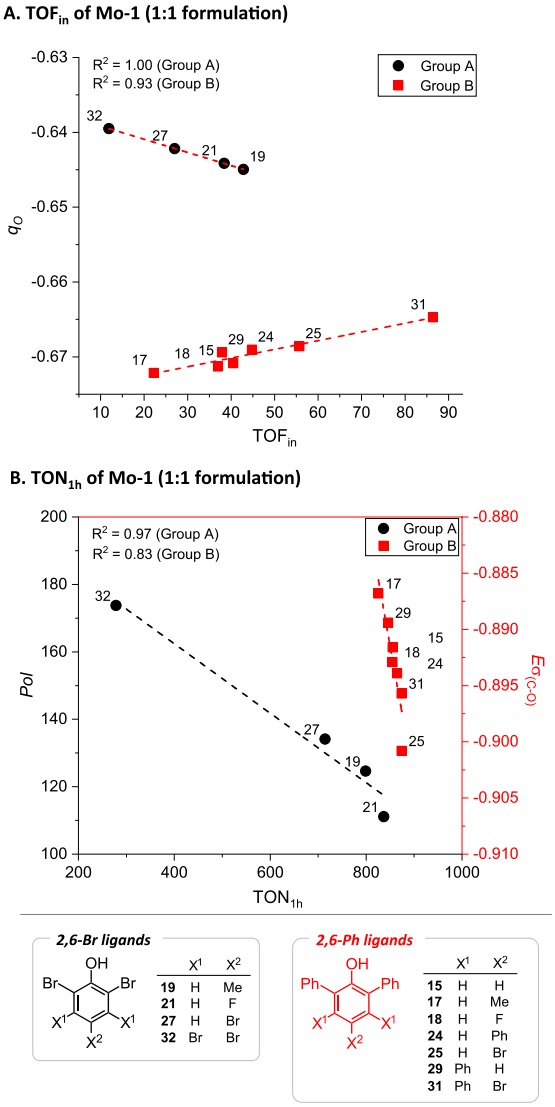

	X^1	X^2
19	H	Me
21	H	F
27	H	Br
32	Br	Br

	X^1	X^2
15	H	H
17	H	Me
18	H	F
24	H	Ph
25	H	Br
29	Ph	H
31	Ph	Br

Figure 5. Univariate correlation of electronic descriptors for selected 1:1 formulations using **Mo-1.**

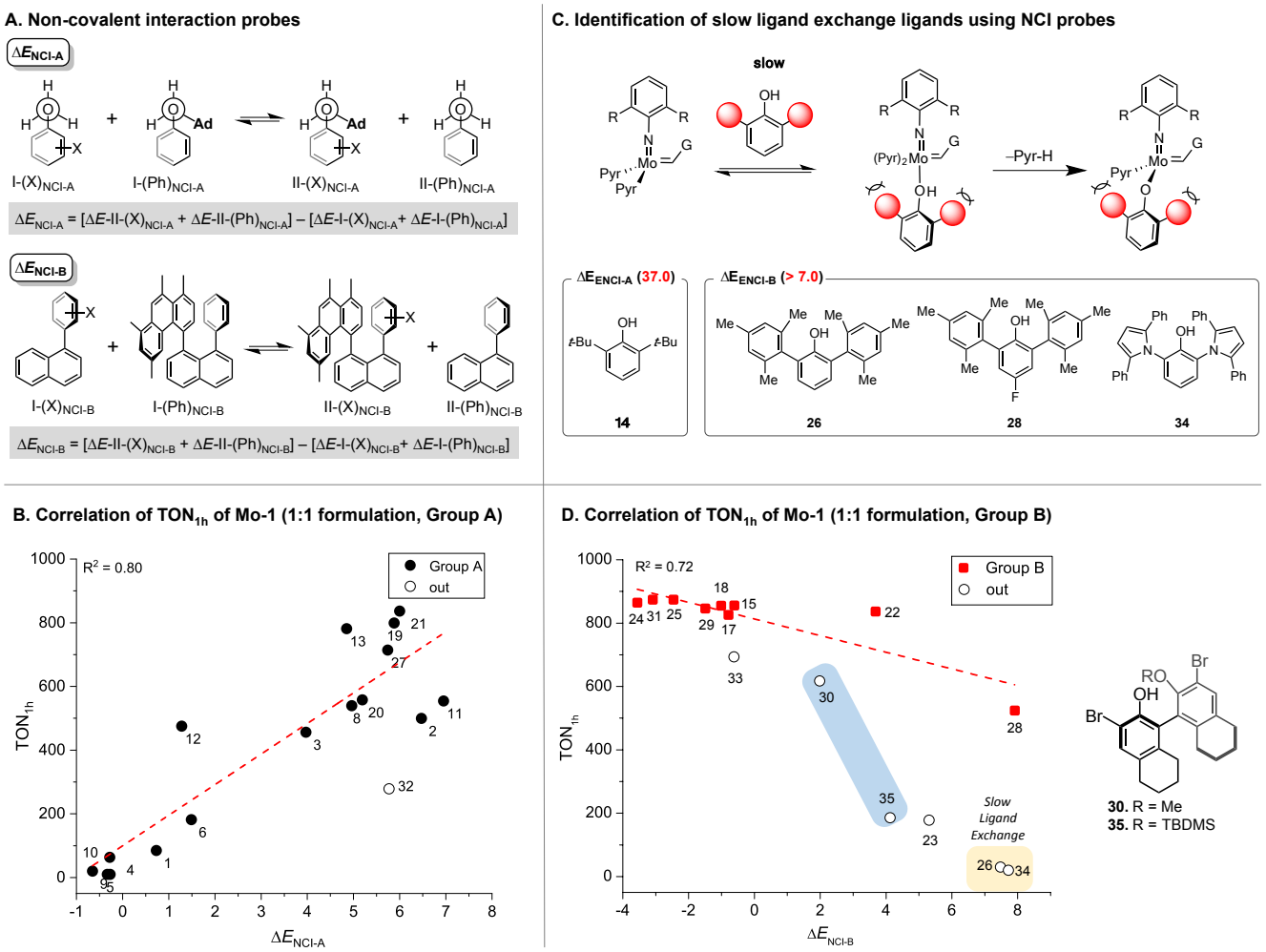

Figure 6. Development of non-covalent interaction probes (A); univariate correlation of TON_{1h} and steric probes for 1:1 formulations with **Mo-1** using $\Delta E_{NCI\text{-}A}$ for Group A phenols (B), and $\Delta E_{NCI\text{-}B}$ for Group B phenols (C, D). Ligand exchange reaction and clustering of slow exchange ligands by using the non-covalent interaction probes (C).

A good correlation (R^2 = 0.80) is found between TON_{1h} (1:1 formulations with **Mo-1**) of Group A, and the $\Delta E_{NCI\text{-}A}$ probe (Figure 6B). Furthermore, good inter-correlations are observed between $\Delta E_{NCI\text{-}A}$ (Group A) and traditional steric parameters ($B_{1,sum}$, $\%V_{bur}$, L_{sum} give $R^2 > 0.9$), while the quality of correlation is moderate to poor with electronic parameters (R^2 = 0.52, 0.39 and < 0.07 for *Pol*, $E\sigma^*_{(C\text{-}O)}$, q_O and $E_{LP(O1)}$, respectively). This suggests that this probe is describing mainly repulsive NCIs (Pauli repulsion). Note that most ligands belonging to Group A gave inactive formulations with the **Mo-2** precursor. This is presumably due to the smaller size of the 2,6-dimethylimido ligand in **Mo-2** compared to 2,6-diisopropylimido ligand in **Mo-1**, which could favor protonation of the alkylidene ligands during exchange[11d] or a faster deactivation pathway due to easier dimerization[27] (see Tables S5 and S6).

We assessed if the new steric probes can be applied to identify phenols undergoing slow exchange with **Mo-1** and **Mo-2** (Figure 6C). One could anticipate that the ligand exchange process proceeds via an associative mechanism similar to that of the olefin coordination to the TBP Mo alkylidene species. The equilibrium between the phenol and the bis-pyrrolide complex (**Mo-1** or **Mo-2**) with the resulting adduct will be dependent on ligand size. The 2,6-(*t*-Bu)$_2$-PhOH (**14**) of Group A does not undergo ligand exchange with **Mo-1** and features a $\Delta E_{NCI\text{-}A}$ value of 37.0, significantly higher than 2,6-(*i*-Pr)$_2$-PhOH (**11**) (7.0). The $\Delta E_{NCI\text{-}B}$ parameter also has demonstrated utility in discriminate slow exchanging ligands of Group B (Figure 6C), identifying bulky ligands (**26**, and **34**) with $\Delta E_{NCI\text{-}B}$ > 7.0 (Figure 6D).

Next, we investigated the applicability of the $\Delta E_{NCI\text{-}B}$ parameter to describe the reactivity of *in situ* formulations with Group B ligands, showing an inverted trend and good correlation with TON_{1h} for phenols in Group B (R^2 = 0.79, Figure 6D). Phenols yielding TON_{1h} > 650 feature negative $\Delta E_{NCI\text{-}B}$ values suggesting the

importance of stabilizing π-stacking and CX---π (X = H, halogen) interactions. However, the subgroup of biaryl ligands, phenols **30** and **35** (Figure 6D) are structurally too different from monoaryl ligands of Group B (and feature an *ortho*-Br substituent) and therefore these phenols did not correlate well with $\Delta E_{NCI\text{-}B}$, despite a qualitative agreement in their observed reactivities. Examining the inter-correlations of the $\Delta E_{NCI\text{-}B}$ descriptor with the other parameter reveals that it has a hybrid character (R^2 = 0.6 for $B_{1,sum}$ and $\%V_{bur}$; 0.2 for *LUMO* and q_H parameters; 0.1 for $E_{LP(O1)\text{-}fenolate}$ and q_O).

Previous studies correlated the rotational barrier about the aryl-naphthalene bond in 1,6-diarylnaphthalenes to σ_{para} parameter, and interpreted this in terms of NCI between the two aryl units.[26] Ultimately, the increase of the substituent size causes a strong repulsive interaction, leading to an increase of $\Delta E_{NCI\text{-}B}$ and corresponding low TON_{1h} values. Notably, the $\Delta E_{NCI\text{-}B}$ parameter does not correlate with phenols in Group A. To summarize, the univariate correlations support our initial hypothesis regarding distinct NCI regimes between phenols of Groups A and B, and the importance of the *ortho* aryl substitution in ArOH ligands.

Aiming to experimentally illustrate the importance of NCI in our catalysts,[28] we found that reaction of trifluorophenol **6** and **Mo-1** in 1:2 ratio yields a dimeric bisaryloxide complex with relatively short contacts between the fluorines and the isopropyl hydrogen atoms (2.4-2.5 Å, Figure S166. These F–H interactions are likely the driving force for the dimer stability, confirming the relevance of NCI for systems described in this work.

In addition, we compared performances of selected 1:1 *in situ* formulations of **Mo-1** to the respective well-defined MAP complexes and selected the most active ligand ArOH **31** and the slow exchanging ligand phenol **26** (Table S7, Figure 7). The catalytic data displays only a minor difference in TOF_{in} and TON_{1h} values for catalysts derived from ArOH **31** showing a modest increase for TOF_{in} with the well-defined MAP catalyst. The performance of the well-defined catalyst obtained from the slowly exchanging ligand ArOH **26** is improved to a slightly higher extent (Figure 7). These results validate the use of catalytic data derived from *in situ* formulations to estimate activity of the respective well-defined MAP complexes.

Multivariate Regression Analysis

As the next step, multivariate linear regression analysis was performed to investigate how the steric and electronic parameters of phenolic ligands could cooperatively impact the TOF_{in} and TON_{1h} responses for Group A and B (Figure 8). We tested the consistency of our models using internal-validation techniques (leave-one-out (LOO) and k-fold methods), yielding good scores for all cases consistent with a well-validated model.[14] The trained models from normalized descriptors gave coefficients that revealed the significance of each of represented effects.

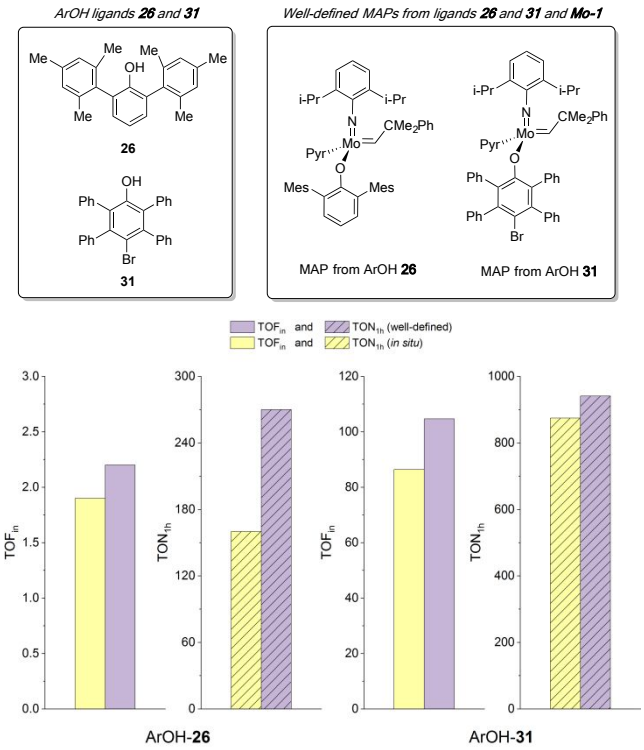

Figure 7. Comparison of 1:1 *in situ* versus well-defined catalysts formulations of **Mo-1** and ligands ArOH **31** and **26** for homodimerization cross-metathesis reaction of 1-nonene.

The multivariate regression analysis for the Group A produced models that describe essentially the same effect for TOF_{in} and TON_{1h} (Figure 8A,B) featuring one steric parameter and one hybrid interaction term, despite failing to incorporate phenols **2** and **11** in the TOF_{in} response. These similarities are consistent with our previous observation that the electronic effect of tested phenols has a minor but not negligible influence on the measured values of TOF_{in} and TON_{1h}. The steric descriptors $\Delta E_{NCI\text{-}A}$ and $\%V_{bur}$ used, respectively, for modelling of TOF_{in} and TON_{1h} describe largely the same effect. The inter-correlation between the $\Delta E_{NCI\text{-}A}$ and $\%V_{bur}$ parameters is R^2 = 0.97. The inclusion of hybrid stereoelectronic descriptors in interaction terms for TOF_{in} (*LUMO* and $B_{5,full}$) and TON_{1h} ($Pol_{phenolate}$ and $E\sigma^*_{(C\text{-}O)}$) describes the properties of the entire ligand associated to the their polarizability ($Pol_{phenolate}$, and $B_{5,full}$ are directly related to polarization). The *LUMO* and $E\sigma^*_{(C\text{-}O)}$ parameters reflect the perturbation of the electron density by pendant substituents with different electronic

properties. However, these terms appear not to be related to the σ-donor ability of the aryloxy ligand, as revealed in Figure 5. It was expected that weaker σ-donor ligands favor TBP- over SP-geometries,[11] increasing the activity and stability of the complex by their lower *trans*-influence.[29]

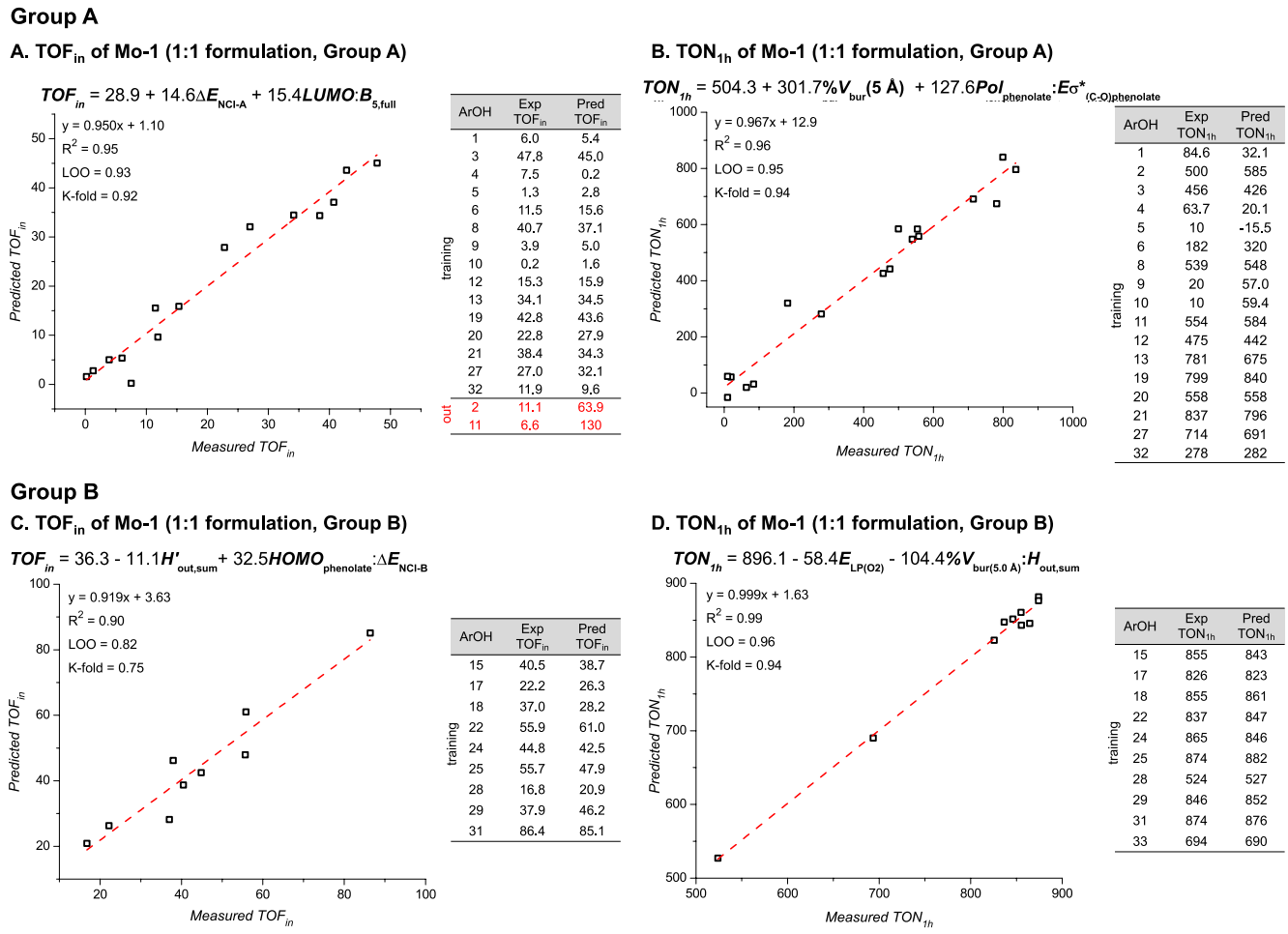

ArOH	Exp TOF$_{in}$	Pred TOF$_{in}$	
1	6.0	5.4	training
3	47.8	45.0	
4	7.5	0.2	
5	1.3	2.8	
6	11.5	15.6	
8	40.7	37.1	
9	3.9	5.0	
10	0.2	1.6	
12	15.3	15.9	
13	34.1	34.5	
19	42.8	43.6	
20	22.8	27.9	
21	38.4	34.3	
27	27.0	32.1	
32	11.9	9.6	
2	11.1	63.9	out
11	6.6	130	

ArOH	Exp TON$_{1h}$	Pred TON$_{1h}$	
1	84.6	32.1	training
2	500	585	
3	456	426	
4	63.7	20.1	
5	10	-15.5	
6	182	320	
8	539	548	
9	20	57.0	
10	10	59.4	
11	554	584	
12	475	442	
13	781	675	
19	799	840	
20	558	558	
21	837	796	
27	714	691	
32	278	282	

ArOH	Exp TOF$_{in}$	Pred TOF$_{in}$	
15	40.5	38.7	training
17	22.2	26.3	
18	37.0	28.2	
22	55.9	61.0	
24	44.8	42.5	
25	55.7	47.9	
28	16.8	20.9	
29	37.9	46.2	
31	86.4	85.1	

ArOH	Exp TON$_{1h}$	Pred TON$_{1h}$	
15	855	843	training
17	826	823	
18	855	861	
22	837	847	
24	865	846	
25	874	882	
28	524	527	
29	846	852	
31	874	876	
33	694	690	

Figure 8. Multivariate linear regression model to predict TOF$_{in}$ and TON$_{1h}$ for Group A (A, B) and Group B (C, D).

However, the performance of catalysts bearing 2,6-(Br)$_2$-substituted phenols in Group A do not fall into this category as revealed by the correlation between TOF$_{in}$ and q_o (Figure 5A).[30] Therefore, these descriptors composing the interaction terms define the stabilizing dispersive forces associated with lower catalytic activity, as exemplified by of the poor performance of pentabromophenol **32**.

Next, ligands of Group B were subjected to the statistical modeling. The correlation found for the TOF$_{in}$ response is notably different to that of Group A. Its significant coefficient in the interaction term (*HOMO*$_{phenolate}$ and Δ*E*$_{NCI-B}$) indicates that it is the defining parameter of the model (Figure 8C), and can be viewed as the σ-donor ability of the phenolate oxygen, described by *HOMO*$_{phenolate}$, as a function of the NCI interactions of the aryl pendants (Δ*E*$_{NCI-B}$). This interaction term is consistent with our empirical observations that weaker σ-donors produced higher catalytic activity, as illustrated by 2,6-(Ph)$_2$- ligands of Group B (Figure 5A). However, this feature can be modulated with the increasing size of the *ortho* substituent, and the steric terms *H'*$_{out,sum}$ and Δ*E*$_{NCI-B}$ introduced in the model reflect the reduction of the activity by the increase of ligand size.

In evaluating the TON$_{1h}$ response, a model was obtained, composed by the electronic parameter *E*$_{LP(O2)}$, and the most significant repulsive interaction term (*%V*$_{bur(5 Å)}$ and *H*$_{out,sum}$) (Figure 8D). The electronic term describes the σ-donor ability of the phenolate oxygen, while the NCI term describes the reduction of activity with the increase of ligand size. Particularly, this model highlights the importance of the substituent size in the stability of the formulation of Group B, in which ligands of comparable size presented similar TON$_{1h}$.

Analysis

To better understand the impact of NCI effects within phenols in the cross metathesis catalytic cycle, we applied a kinetic model similar to that of Kozuch and Shaik, who defined how the TOF of a catalytic system can be calculated from the energy span (δ*E*, in our case ΔΔG) between the most stable intermediate and the highest energy transition state of a catalytic cycle, to a small subset of ligands of Group A (**4**, **6**, **13**, **20**, **27**).[31] Thus, energies of TBP and SP metallacycle geometries, recognized as the resting state intermediates of olefin cross metathesis, were calculated revealing a good correlation between TOF_{in} and the lowest energy metallacycles (Figure 9A). Steric effects destabilize both penta-coordinated metallacycle intermediates, reducing the energy span (δ*E*) of the overall reaction and therefore increasing the catalytic activity (reaction rate). However, very bulky (aryloxide) ligands destabilize the TBP isomers less than off-cycle SP isomers because bulkier aryloxide ligands are better accommodated in the apical position of TBP intermediates for most imido ligands.[32] This preference for the TBP geometry with increasing steric properties of the aryloxide ligands is evident for both Groups A and B of calculated complexes (Table S16) and is in line with trends revealed by the DEACT parameter, where more stable catalysts are associated with large aryloxide ligands. Alternatively, the energy of the rate-determining transition state of the catalytic cycle correlates with the stability of these intermediates. Previous calculations revealed that the cycloreversion step has the highest Gibbs free energy barrier on the productive pathway of olefin metathesis.[6]

To test both hypotheses, we used previous computational results involving the productive pathway of olefin metathesis for MAP Mo and W d^0 alkylidenes catalysts,[6c] and found a strong correlation (R^2 = 0.82) between the calculated relative energies of TBP-isomers of W and Mo complexes with different alkoxy ligands and energy barriers of the cycloreversion step ΔΔG‡. That said, no correlation is found using the transition state energy ΔG‡ (R^2 = 0.05) (Figure 9B). We speculate that the size of substituents in aryloxy ligands could influence, via NCI effects, the cycloreversion transition state to a much less extent than the TBP/SP geometries, due to its late character, explaining the previous correlations. We conclude that for Group A, the changes caused by NCI in the energy span (δ*E*) between the cycloreversion step and the resting state intermediates have the main contribution from the energies of metallacyclobutanes.

As for Group B, two selected phenols (**15** and **26**) did not follow the trend observed for TBP-SP metallacycles of Group A. This result is not unexpected considering the inverse linear trend between the two groups (Figure 4C). The aryl arms on phenols of Group B generate CX---π (X = H, halogen) NCI, which are of distinct nature compared to Group A (Pauli repulsion). The most active catalysts of Group B feature higher stabilizing NCIs ($\Delta E_{NCI\text{-}B}$ <0, Figure 6C), which possibly reduce the energy barrier of the cycloreversion step. In contrast to ligands of Group A, the ligands of Group B are large enough to significantly influence the energy of the transition state of the cycloreversion step through the NCIs. These NCIs are increased by pendant -Ph (*meta* and *para*) and -Br (*para*) substituents in 2,6-$(Ph)_2$-ArOH. However, the increase of sterics by bulkier *ortho*-pendants leads to a drastic drop in catalytic performance, as also discussed before for some bulkier phenols with $\Delta E_{NCI\text{-}B}$ >0, where the ligand exchange step is too slow.

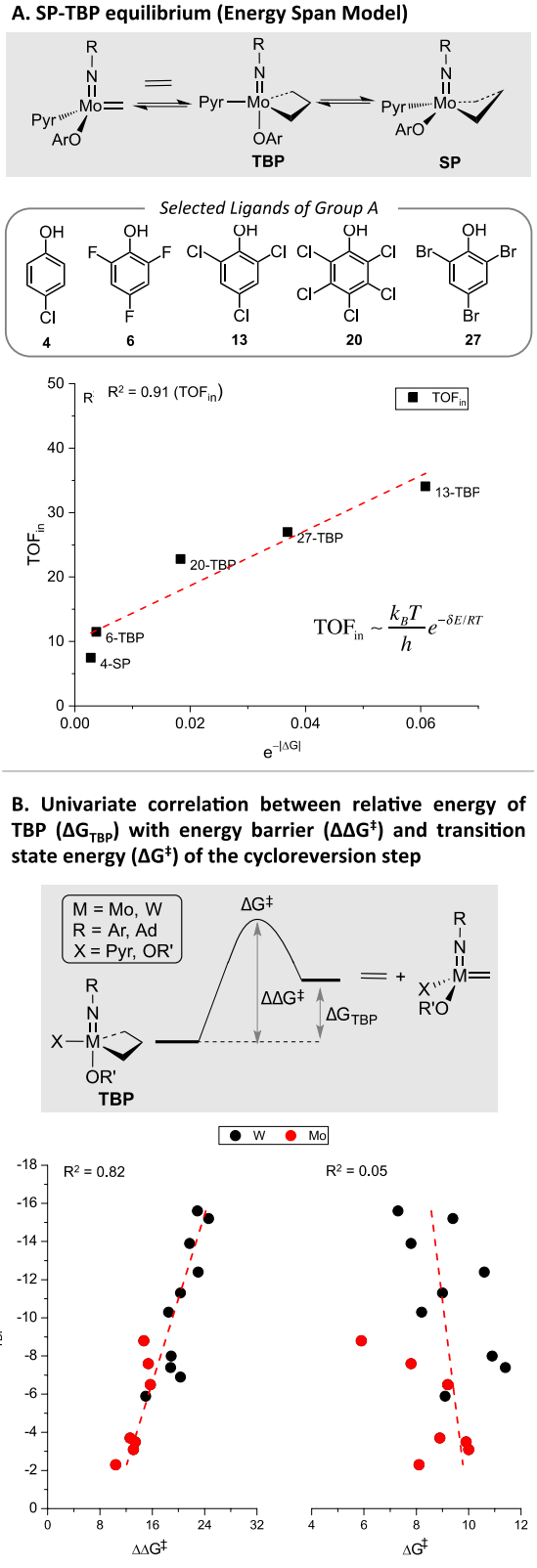

Figure 9. (A) Linear correlation between TOF_{in} and TON_{1h} with $e^{-|\Delta G|}$ where ΔG of the lowest energy conformer was considered. Pyr = 2,5-dimethylpyrrolide. (B) Univariate correlations between the cycloreversion step energies and the TBP metallacycle. For panel B, data taken from ref 6c.

CONCLUSIONS

We have demonstrated that the efficiency of the MAP Mo imido alkylidene metathesis catalysts depends on the NCIs exerted by the aryloxy substituent ligands. Using statistical tools, we categorized the data set of 35 phenols into two groups and provided evidence that NCIs define catalysis: Group A containing phenols without aryl arms in the *ortho* position (**1**-**14**, **16**, **19**-**21**, **27**, **32**), and Group B with *ortho*-arylated phenols (**15**, **17**-**18**, **22**-**26**, **28**-**31**, **33**-**35**). Overall catalytic performances of *in situ* prepared MAP catalysts with ligands of both Group A and B (as evaluated by TON_{1h}) is dominated, respectively, by repulsive and attractive interactions (NCI), showing opposite trends with the increase of the *ortho* pendant substituent size. Energetic span analysis suggests an intrinsic relationship between NCIs and the cycloreversion step. Specifically group A ligands influence the energy of SP/TPB resting states intermediates, while Group B ligands mainly impact the transition state energy for the cycloreversion step. The initial rates (TOF_{in}) are also influenced by an electronic effect of phenol ligands that is more pronounced for 2,6-$(Br)_2$- derivatives and 2,6-$(Ph)_2$- derivatives, although with different trends: 2,6-$(Br)_2$- phenol derivatives display decreasing initial rates with increasing electronegativity (reduced σ donation ability), but the opposite is observed for 2,6-$(Ph)_2$- derivatives. While research efforts in ligand design for MAP Mo imido alkylidene metathesis catalysts have so far mainly focused on the σ-donation ability of ligands, this work uncovers that the NCI is the key driver for high catalyst activity in the cross-metathesis reaction with d^0 catalysts. To conclude, although this work focused on a homodimerization cross-metathesis reaction, we believe that the main conclusions can guide catalyst selection in other cross-metatheses reactions and related macrocyclic ring-closing metatheses reactions.

AUTHOR INFORMATION

Corresponding Author

marco.ferreira@ufscar.br
fedoroal@ethz.ch
matt.sigman@utah.edu
ccoperet@ethz.ch

Author Contributions

The manuscript was written through contributions of all authors. All authors have given approval to the final version of the manuscript.

ACKNOWLEDGMENT

The authors are grateful to the Scientific Equipment Program of ETH Zürich and the SNSF (R'Equip grant 206021_150709/1) for financial support of the high throughput catalyst screening facility (HTE@ETH). M.A.B.F thanks Fundação de Amparo à Pesquisa do Estado de São Paulo (FAPESP, proc. n° 17/13306-1, 15/08541-6 and 14/50249-8) for financial support. J.D.J.S. was supported by the National Research Fund, Luxembourg (AFR Individual Ph.D. Grant 12516655). M.S.S. thanks the National Science Foundation (CHE-1763436) for support. The support and resources from the Center for High Performance Computing at the University of Utah are gratefully acknowledged. The authors thank XiMo Hungary Ltd for donation of **Mo**-**1**,**2** and selected phenol ligands.

SUPORTING INFORMATION

Experimental procedures, catalytic data, plots of conversion vs. time and selectivity vs. time for catalytic experiments, NMR spectra, modeling details, and Cartesian coordinates.

REFERENCES

1. (a) Grubbs, R. H., Ed.; Handbook of Metathesis; Wiley-VCH: Weinheim, Germany, 2014. (b) Higman, C. S.; Lummiss, J. A. M.; Fogg, D. E. Olefin Metathesis at the Dawn of Implementation in Pharmaceutical and Specialty-Chemicals Manufacturing. *Angew. Chem., Int. Ed.* **2016**, *55*, 3552.
2. Jiang, A. J.; Zhao, Y.; Schrock, R. R.; Hoveyda, A. H. Highly *Z*-Selective Metathesis Homocoupling of Terminal Olefins. *J. Am. Chem. Soc.* **2009**, *131*, 16630.
3. (a) Copéret, C.; Allouche, F.; Chan, K. W.; Conley, M. P. D.; Murielle F.; Fedorov, A.; Moroz, I. B.; Mougel, V.; Pucino, M.; Searles, K.; Yamamoto, K.; Zhizhko, P. A. Bridging the Gap between Industrial and Well-Defined Supported Catalysts. *Angew. Chem. Int. Ed.* **2018**, *57*, 6398. (b) Hoveyda, A. H. Evolution of Catalytic Stereoselective Olefin Metathesis: From Ancillary Transformation to Purveyor of Stereochemical Identity. *J. Org. Chem.*, **2014**, *79*, 4763.
4. Meek1, S. J.; O'Brien, R. V.; Llaverial, J.; Schrock, R. R.; Hoveyda, A. H. Catalytic *Z*-selective olefin cross-metathesis for natural product synthesis. *Nature*, **2011**, *471*, 461.
5. (a) Koh, M. J.; Nguyen, T. T.; Lam, J. K.; Torker, S.; Hyvl, J.; Schrock, R. R.; Hoveyda, A. H. Molybdenum chloride catalysts for *Z*-selective olefin metathesis reactions. *Nature* **2017**, *542*, 80. (b) Lam, J. K.; Zhu, C.; Bukhryakov, K. V.; Müller, P.; Hoveyda, A. H.; Schrock, R. R. Synthesis and Evaluation of Molybdenum and Tungsten Monoaryloxide Halide Alkylidene Complexes for *Z*-Selective Cross-Metathesis of Cyclooctene and *Z*-1,2-Dichloroethylene. *J. Am. Chem. Soc.* **2016**, *138*, 15774.
6. (a) Solans-Monfort, X.; Clot, E.; Copeŕet, C.; Eisenstein, O. d^0 Re-Based Olefin Metathesis Catalysts, Re(≡CR)(=CHR)(X)(Y): The Key Role of X and Y Ligands for Efficient Active Sites. *J. Am. Chem. Soc.* **2005**, *127*, 14015. (b) Solans-Monfort, X.; Copeŕet, C.; Eisenstein, O. Oxo vs Imido Alkylidene d^0-Metal Species: How and Why Do They Differ in Structure, Activity, and Efficiency in Alkene Metathesis? *Organometallics*, **2012**, *31*, 6812. (c) Solans-Monfort, X.; Copeŕet, C.; Eisenstein, O. Metallacyclobutanes from Schrock-Type d^0 Metal Alkylidene Catalysts: Structural Preferences and Consequences in Alkene Metathesis. *Organometallics*, **2015**, *34*, 1668. (d) Poater, A; Solans-Monfort, X; Clot, E.; Copéret, C.; Eisenstein, O. Understanding d^0-Olefin Metathesis Catalysts: Which Metal, Which Ligands? *J. Am. Chem. Soc.* **2007**, *129*, 8207.
7. (a) Hérisson, J. L.; Chauvin, Y. Catalyse de transformation des oléfines par les complexes du tungstène. II. Télomérisation des oléfines cycliques en présence d'oléfines acycliques. *Makromol. Chem.* **1971**, *141*, 161. (b) Chauvin, Y. Olefin Metathesis: The Early Days (Nobel Lecture). *Angew. Chem., Int. Ed.* **2006**, *45*, 3740.
8. Gordon, C. P.; Yamamoto, K.; Liao, W.-C.; Allouche, F.; Andersen, R. A.; Copéret, C.; Raynaud, C.; Eisenstein, O. Metathesis Activity Encoded in the Metallacyclobutane Carbon-13 NMR Chemical Shift Tensors. *ACS Cent. Sci.* **2017**, *3*, 759.
9. Solans-Monfort, X.; Copeŕet, C.; Eisenstein, O. Shutting Down Secondary Reaction Pathways: The Essential Role of the Pyrrolyl Ligand in Improving Silica Supported d^0-ML_4 Alkene Metathesis Catalysts from DFT Calculations. *J. Am. Chem. Soc.* **2010**, *132*, 7750.
10. Leduc, A.-M.; Salameh, A.; Soulivong, D.; Chabanas, M.; Basset, J.-M.; Copéret, C.; Solans-Monfort, X.; Clot, E.; Eisenstein, O.; Böhm, V. P. W.; Röper, M. β-H Transfer from the Metallacyclobutane: A Key Step in the Deactivation and Byproduct Formation for the Well-Defined Silica-Supported Rhenium Alkylidene Alkene Metathesis Catalyst. *J. Am. Chem. Soc.*, **2008**, *130*, 6288.
11. (a) Jiang, A. J.; Simpson, J. H.; Müller, P.; Schrock, R. R. Fundamental Studies of Tungsten Alkylidene Imido Monoalkoxidepyrrolide Complexes. *J. Am. Chem. Soc.* **2009**, *131*, 7770. (b) Flook, M. M.; Jiang, A. J.; Schrock, R. R.; Müller, P.; Hoveyda, A. H. *Z*-Selective Olefin Metathesis Processes Catalyzed by a Molybdenum Hexaisopropylterphenoxide Monopyrrolide Complex. *J. Am. Chem. Soc.* **2009**, *131*, 7962. (c) Schrock, R. R.; Jiang, A. J.; Marinescu, S. C.; Simpson, J. H.; Möller, P. Fundamental Studies of Molybdenum and Tungsten Methylidene and Metallacyclobutane Complexes. *Organometallics* **2010**, *29*, 5241. (d) Mougel, V.; Copéret, C. Magnitude and consequences of OR ligand σ -donation on alkene metathesis activity in d^0 silica supported (≡SiO)W(NAr)(=CHtBu)(OR) catalysts. *Chem. Sci.* **2014**, *5*, 2475.
12. (a) Hock, A. S.; Schrock, R. R.; Hoveyda, A. H. Dipyrrolyl Precursors to Bisalkoxide Molybdenum Olefin Metathesis Catalysts. *J. Am. Chem. Soc.* **2006**, *128*, 16373. (b) Singh, R.; Schrock, R. R.; Müller, P.; Hoveyda, A. H. Synthesis of Monoalkoxide Monopyrrolyl Complexes Mo(NR)(CHR')(OR' ')(pyrrolyl): Enyne Metathesis with High Oxidation State Catalysts. *J. Am. Chem. Soc.* **2007**, *129*, 12654. (c) Jiang, A. J.; Zhao, Y.; Schrock, R. R.; Hoveyda, A. H. Highly *Z*-Selective Metathesis Homocoupling of Terminal Olefins. *J. Am. Chem. Soc.* **2009**, *131*, 16630.
13. (a) Mougel, V.; Santiago, C. B.; Zhizhko, P. A.; Bess, E. N.; Varga, J.; Frater, G.; Sigman, M. S.; Copeŕet, C. Quantitatively Analyzing Metathesis Catalyst Activity and Structural Features in Silica-Supported Tungsten Imido–Alkylidene Complexes. *J. Am. Chem. Soc.* **2015**, *137*, 6699.

(b) Engl, P. S.; Santiago, C. B.; Gordon, C. P.; Liao, W.-C.; Fedorov, A., Copeŕet, C.; Sigman, M. S.; Togni, A. Exploiting and Understanding the Selectivity of Ru-N-Heterocyclic Carbene Metathesis Catalysts for the Ethenolysis of Cyclic Olefins to α,ω-Dienes. *J. Am. Chem. Soc.* **2017**, *139*, 13117.

14. Zhizhko, P. A.; Mougel, V.; Silva, J. J. Copéret, C. Benchmarked Intrinsic Olefin Metathesis Activity: Mo vs. W. *Helv. Chim. Acta* **2018**, *101*, e1700302.
15. Singh, R. Cyclopropene Polymerization and Enyne Metathesis Catalyzed by High Oxidation State Molybdenum Alkylidenes. PhD thesis. Massachusetts Institute of Technology, **2008**.
16. (a) Guo, J.-Y.; Minko, Y.; Santiago, C. B.; Sigman, M. S. Developing Comprehensive Computational Parameter Sets To Describe the Performance of Pyridine-Oxazoline and Related Ligands. *ACS Catal.* **2017**, *7*, 4144. (b) Santiago, C. B.; Guo, J.-Y.; Sigman, M. S. Predictive and mechanistic multivariate linear regression models for reaction development. *Chem. Sci.*, **2018**, *9*, 2398.
17. (a) Santiago, C. B.; Milo, A.; Sigman, M. S. Developing a Modern Approach To Account for Steric Effects in Hammett-Type Correlations. *J. Am. Chem. Soc.* **2016**, *138*, 13424. (b) Hollingsworth, C. A.; Seybold, P. G.; Hadad, C. M. Substituent effects on the electronic structure and pKa of benzoic acid. *Int. J. Quantum Chem.* **2002**, *90*, 1396.
18. Verloop, A. in *Drug Design*, E. J. Ariens, Ed. (Academic Press, 1976), vol. 3, pp. 133–187.
19. Sevov, C. S.; Hickey, D. P.; Cook, M. E.; Robinson, S. G.; Barnett, S.; Minteer, S. D.; Sigman, M. S.; Sanford, M. S. Physical Organic Approach to Persistent, Cyclable, Low-Potential Electrolytes for Flow Battery Applications. *J. Am. Chem. Soc.*, **2017**, *139*, 2924.
20. (a) Hillier, A. C.; Sommer, W. J.; Yong, B. S.; Petersen, J. L.; Cavallo, L.; Nolan, S. P. A Combined Experimental and Theoretical Study Examining the Binding of *N*-Heterocyclic Carbenes (NHC) to the Cp*RuCl (Cp* = η^5-C_5Me_5) Moiety: Insight into Stereoelectronic Differences between Unsaturated and Saturated NHC Ligands. *Organometallics* **2003**, *22*, 4322. (b) Clavier, H.; Nolan, S. P. Percent buried volume for phosphine and *N*-heterocyclic carbene ligands: steric properties in organometallic chemistry. *Chem. Commun.* **2010**, *46*, 841.
21. Toste, F. D.; Sigman, M. S.; Miller, S. J. Pursuit of Noncovalent Interactions for Strategic Site-Selective Catalysis. *Acc. Chem. Res.* **2017**, 50, 609.
22. (a) Orlandi, M.; Hilton, M. J.; Yamamoto, E.; Toste, F. D.; Sigman, M. S. Mechanistic Investigations of the Pd(0)-Catalyzed Enantioselective 1,1-Diarylation of Benzyl Acrylates. *J. Am. Chem. Soc.* **2017**, *139*, 12688. (b) Orlandi, M.; Coelho, J. A. S.; Hilton, M. J.; Toste, F. D.; Sigman, M. S. Parametrization of Non-covalent Interactions for Transition State Interrogation Applied to Asymmetric Catalysis. *J. Am. Chem. Soc.*, **2017**, *139*, 6803.
23. (a) Neel, A. J.; Hilton, M. J.; Sigman, M. S.; Toste, F. D. Exploiting non-covalent π interactions for catalyst design. *Nature*, **2017**, *543*, 637. (b) Wagner, J. P.; Schreiner, P. R. London Dispersion in Molecular Chemistry—Reconsidering Steric Effects. *Angew. Chem. Int. Ed.* **2015**, *54*, 12274.
24. Bohm, S.; Exner, O. Steric effects of polar substituents evaluated in terms of energy by means of isodesmic reactions. *Org. Biomol. Chem.* **2008**, *6*, 1092.
25. Wheeler, S. E.; Houk, K. N.; Schleyer, P. v. R.; Allen, W. D. A Hierarchy of Homodesmotic Reactions for Thermochemistry. *J. Am. Chem. Soc.*, **2009**, *131*, 2547.
26. Cozzi, F.; Cinquini, M.; Annuziata, R.; Dwyer, T.; Siegel, J. Polar/.pi. interactions between stacked aryls in 1,8-diarylnaphthalenes. *J. Am. Chem. Soc.* **1992**, *114*, 5729.
27. (a) Robbins, J.; Bazan, G. C.; Murdzek, J. S.; O'Regan, M. B.; Schrock, R. R. Reduction of molybdenum imido-alkylidene complexes in the presence of olefins to give molybdenum(IV) complexes. *Organometallics* **1991**, *10*, 2902. (b) Lopez, L. P. H.; Schrock, R. R.; Müller, P. Dimers that Contain Unbridged W(IV)/W(IV) Double Bonds. *Organometallics* **2006**, 25, 1978.
28. Sinha, A.; Lopez, L. P. H.; Schrock, R. R.; Hock, A. S.; Müller, P. Reactions of M(N-2,6-i-$Pr_2C_6H_3$)(CHR)(CH_2R')$_2$ (M = Mo, W) Complexes with Alcohols To Give Olefin Metathesis Catalysts of the Type M(N-2,6-i-$Pr_2C_6H_3$)(CHR)(CH_2R')(OR' '). *Organometallics* **2006**, *25*, 1412.
29. Coe, B. J.; Glenwright, S. J. Trans-effects in octahedral transition metal complexes. *Coord. Chem. Rev.* **2000**, *203*, 5.
30. The interaction between *ortho*-Br substituent in an aryloxy ligand and Mo (Mo---Br) was demonstrated, see: Meek, S. J.; Malcolmson, S. J.; Li, B.; Schrock, R. R.; Hoveyda, A. H. The Significance of Degenerate Processes to Enantioselective Olefin Metathesis Reactions Promoted by Stereogenic-at-Mo Complexes. *J. Am. Chem. Soc.* **2009**, *131*, 16407.
31. Kozuch, S.; Shaik, S. A Combined Kinetic−Quantum Mechanical Model for Assessment of Catalytic Cycles: Application to Cross-Coupling and Heck Reactions. *J. Am. Chem. Soc.* **2006**, *128*, 3355.
32. (a) Gerber, L. C. H.; Schrock, R. R.; Müller, P. Molybdenum and Tungsten Monoalkoxide Pyrrolide (MAP) Alkylidene Complexes That Contain a 2,6-Dimesitylphenylimido Ligand. *Organometallics* **2013**, *32*, 2373. (b) Axtell, J. C.; Schrock, R. R.; Müller, P.; Hoveyda, A. H. Synthesis of Molybdenum and Tungsten Alkylidene Complexes That Contain the 2,6-Bis(2,4,6-triisopropylphenyl)phenylimido (NHIPT) Ligand. *Organometallics* **2015**, *34*, 2110.

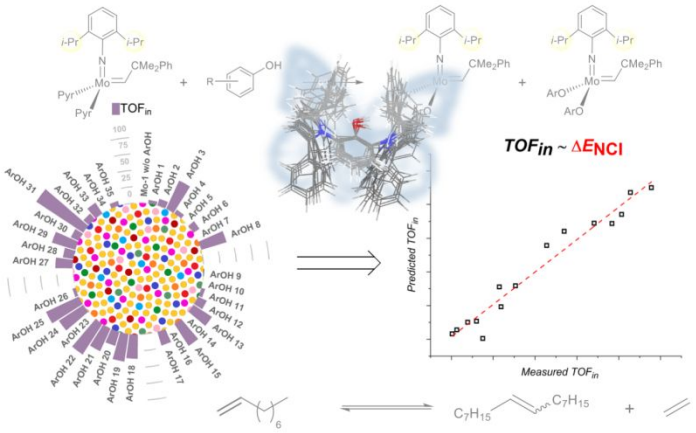
TOF$_{in}$
Mo-1 w/o ArOH
ArOH 1
ArOH 2
ArOH 3
ArOH 4
ArOH 5
ArOH 6
ArOH 7
ArOH 8
ArOH 9
ArOH 10
ArOH 11
ArOH 12
ArOH 13
ArOH 14
ArOH 15
ArOH 16
ArOH 17
ArOH 18
ArOH 19
ArOH 20
ArOH 21
ArOH 22
ArOH 23
ArOH 24
ArOH 25
ArOH 26
ArOH 27
ArOH 28
ArOH 29
ArOH 30
ArOH 31
ArOH 32
ArOH 33
ArOH 34
TOF$_{in}$ ~ ΔE$_{NCI}$
Predicted TOF$_{in}$
Measured TOF$_{in}$
C$_7$H$_{15}$
C$_7$H$_{15}$